Physics of the Solid State, 2024, Vol. 66, No. 5

08,10

Effect of deformation on the radiation formation of interlayer bridges in bilayer graphene

© *A.I. Podlivaev* [1,2]

[1] National Research Nuclear University, „MEPhI“,
Moscow, Russia
[2] Research Institute of Problems in the Development of Scientific
and Educational Potential of Young People,
Moscow, Russia
E-mail: AIPodlivayev@mephi.ru

Received February 26, 2024
Revised February 26, 2024
Accepted March 20, 2024

Within the framework of the non-orthogonal tight-binding model, the influence of uniform stretching of bilayer graphene on the process of radiation formation of interlayer bridges in this structure was studied. Model calculations have shown that stretching bilayer graphene by 5% increases the total probability of the formation of defects of all types by ~ 2 times. It is shown that the proportion of structures with interlayer bridges that have sufficient thermal stability for long-term existence at room temperature does not depend on deformation. In deformed and undeformed bilayer graphene, this fraction is $\sim 15\%$. One of the found stable structures with an interlayer bridge is a type of Frenkel pair and has an annealing activation energy of 2.11 eV. In earlier work, when simulating the irradiation of undeformed bilayer graphene within a similar model, this defect was not observed

Keywords: Bilayer graphene, radiation defects, interlayer bridges, deformation, molecular dynamics.

DOI: 10.61011/PSS.2024.05.58505.63

1. Introduction

Properties of a planar structure — graphene [1] — with high carrier mobility [2] and unique strength [3] may be effectively controlled by combining graphene with planar structures as well as with individual elements and molecules. Such adaptation of graphene monolayer properties is currently extensively investigated because it can be applicable for creation of graphene electronic components such as transistors, microcapacitors, biosensors, etc. (see,for example, [4–8]). Practical capability to control mechanical and electronic properties activated the search for planar structures that are closely related to graphene and consisting of one or several atomic layers. Thus, in 2019, a bilayer „graphene–borophene“ structure [9] with high heterostructure resistance and elasticity was synthesized and may be suitable for opto- and acousto-electronics applications [10,11]. Diaman — a bilayer nanostructure with interlayer covalent bonds was predicted [12] and later synthesized [13]. Theoretical studies have shown that diaman may be used in optoelectronic devices [14]. Bilayer graphene (BG) is the initial material for diaman synthesis and may be also used in graphene electronic components. Thus, [15] described BG synthesis and showed the capability to control band gap. Capability to control bandgap by a vertical electric field makes BG a promising material for creating a new type of transistors [16,17]. BG may be used as a humidity sensor [18] and toxic gas adsorbent [19]. Potential applicability of defect bilayer graphene as a biosensor is shown in [20]

Controlled covalent interlayer bonding expands the range of possible BG applications considerably. Formation of a maximum permissible number of bonds transforms the BG structure to diaman. Prospects of application of perforated graphene structures with interlayer bridges in electronics were shown in [21] within the framework of the density functional theory (DFT). Possible utilization of such structures as hydrogen accumulators was addressed.

Study [22] uses statistical and dynamic simulation to investigate formation of interlayer bridges in BG when exposed to irradiation, and thermal stability of these bridges. Simulation in [22] was performed using the nonorthogonal tight-binding model — NTBM, [23]) with dispersion corrections [24] that allow interlayer interaction in graphite and bilayer graphene to be adequately considered. Study [22] showed that interlayer bridges may really occur in the BG structure exposed to irradiation. The kind od damage in the BG structure differs from that of graphite.

Considerable damage of both graphene planes near the bridge is a common feature of all found defect BG configurations. However, the efficiency of formation of thermally stable bridges was low. Most of ($\sim 85\%$) the generated bridges had low thermal stability that prevented their practical application. The main reason why these configurations are unstable is that the primary knocked-on atom (PKA) at rest is in close proximity to its initial location in the undamaged BG. The objective of this study was to identify the features of radiation-induced generation of interlayer bridges in uniformly stretched BG. The interest in investigating the deformation effects is induced by two reasonable assumptions.

First, transverse stretching of BG planes will increase resistance of each graphene plane to transverse displacement. Such displacement causes PKA channeling between the planes. Reduction of displacements suppresses the PKA energy transfer to the surrounding crystal, thus, PKA moves away at a longer distance from the initial location and the arising defect may be more stable. This assumption is indirectly supported by the calculations in [22]. This study (where PKA paths in graphite and BG are compared at equal initial velocities) shows that the PKA path in graphite is higher due to high resistance to transverse displacement of graphite planes.

Second, stretching simplifies formation of the necessary damage of both planes, therefore, bridge (including thermally stable) formation probability is increased.

2. Calculation methods

Similar to [22], the tight-binding approximation has been chosen for the simulation [23,24]. Software implementation of NTBM potential [23] is published in [25]. Results of this approach match well with the DFT data for structures containing carbon atoms in states with various types of hybridization [26]. This model was successfully used to study numerous systems consisting of carbon, hydrogen, nitrogen and oxygen atoms (see, for example, [22–26] and reference therein).

BG was examined using a 2×2 C_{128} supercell consisting of two C_{64} layers (see [34]). Cartesian positions have been chosen in such a way that the BG layers are perpendicular to the Z axis. Figure 1 shows frontal view of the computational cell with Cartesian and spherical positions. The initial cell shape is identical to that taken in [22], where a side view of the cell is also shown.

The calculations used two types of periodic boundary conditions. Translation vectors of *Vstress* structure that is unstrained V_0 and uniformly stretched in (X, Y) directions are equal to $(13.241, 0, 0)$, $(1.918, 13.101, 0)$, $(0, 0, \infty)$ and $(13.903, 0, 0)$, $(2.014, 13.756, 0)$, $(0, 0, \infty)$ (Å), respectively. Study [28] (conducted using a similar NTBM potential) reports that uniform stretching within 5% is elastic and such strain is far from ultimate strain that causes structure failure.

Initial atom positions corresponded to the unstrained BG structure *Vstress* (see Figure 1). Initial interatomic forces were equal to zero, while the initial velocities were equal to zero, except the velocity of a single PKA. Two non-equivalent options were addressed — an atom with $N_r = 1$ or $N_r = 2$ was chosen as PKA (see Figure 1). Zenith angle Θ of the initial PKA velocity directions was equal to $(4/6,\ 5/6,\ 6/6) \times \pi$. Azimuth angle φ was equal to $(0/4,\ 1/4,\ 2/4,\ 3/4,\ 4/4) \times \pi$. The initial kinetic energy E_0 of PKA was equal to 21, 24, 27, 30, 33, 36 and 39 eV.

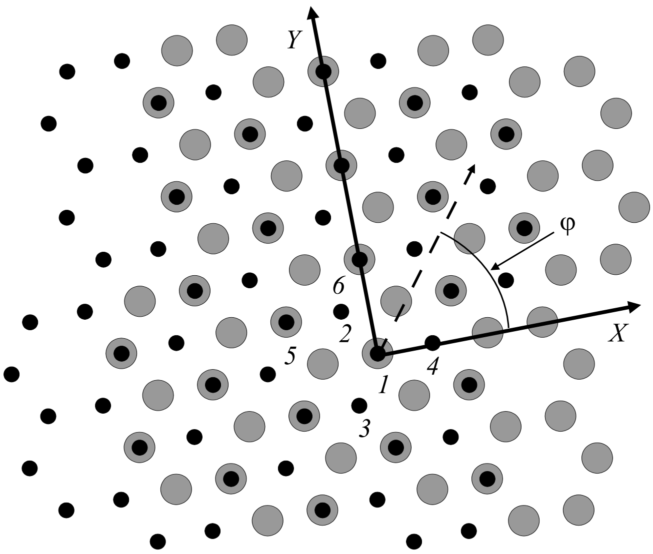

Figure 1. Computational BG cell BG consisting of 128 atoms (plan view). Grey large balls show the bottom graphene plane (64 atoms), black small balls show the top graphene plane (64 atoms).

Herein as well as in [22], dynamic simulation, formation of radiation-induced defects were performed within a microcanonical assembly [35]. The Verlet algorithm with time step size 0.3 fs was used. Dynamic simulation was performed for 3000 time steps that corresponds to real time ~ 1 ps. After completion of the dynamic defect formation phase, the structure was brought back to unstretched state V_0 by uniform compression. After that, the potential energy was minimized on all atom positions. This approach is used to identify identical types of radiation-induced defects formed in initially strained and unstrained crystals. To compare the properties of the radiation-induced defects, the following quantities were defined: E_{rel} — energy of this defect at zero temperature (Wigner energy). E_a — annealing activation energy of this defect. A — frequency factor in the following Arrhenius equation

$$\tau^{-1}(T) = A \exp(-E_a/k_{\text{B}}T), \tag{1}$$

where T is the temperature, k_{B} is Boltzmann's constant. *Dist* is the distance from PKA in a finite defect state to the vacancy center in the top BG plane. Let us denote the radius vector of the vacancy center as $\mathbf{R}_{\text{vac}}$. If an atom with $N_r = 1$ is the primary knocked-on atom (see Figure 1), then $\mathbf{R}_{\text{vac}} = (\mathbf{R}_2 + \mathbf{R}_3 + \mathbf{R}_4)/3$, where $\mathbf{R}_i$ is the radius vector of the corresponding vacancy boundary atom. For PKA with $N_r = 2$, $\mathbf{R}_{\text{vac}} = (\mathbf{R}_1 + \mathbf{R}_5 + \mathbf{R}_6)/3$.

Software package [25] and new algorithm of search for saddle points between two stable states [36] are used to study most probable system paths during defect annealing. Saddle configurations in the joint coordinate space are defined to find the annealing activation energy E_a. Frequency factor A in equation (1) was calculated using the

Vineyard equation [37]) from phonon spectra of the system in a metastable defect state and saddle point. Variable $N_{\text{coord}} = \text{C2, C3}$ denotes the number of covalent bonds of the atom (two and three bonds, respectively) that forms a bridge between graphene planes with atoms of these planes.

3. Findings and discussion

Like in [22], only local defects with short distance between PKA and the formed vacancy ($Dist < 4\,\text{Å}$) were studied in detail. At these values of Dist, the most energetically favorable configurations of spiro interstitial atoms were not observed. A spiro interstitial atom [38]) is located between the adjacent graphite or BG planes and is covalently bonded with two carbon atoms of the top atomic plane and two atoms of the bottom atomic plane. Defect configurations found herein partially coincide with configurations described in [22] and hereinafter (in the main text) are denote as: B1-B10, Decay, I1, I2. There are interlayer bridges in B1-B10 (Bridge) configurations. Decay symbol denotes a configuration where one atom moves away, as result of radiation-induced impact, from the rest structure at a distance that avoids interatomic interaction. In 24 observations of this defect, the atom moved away from the PKA structure, and only in three cases PKA (with central impact) transferred its energy to another atom that later separated rom the structure. The total number of defects M of all types with some main properties are listed in the table.

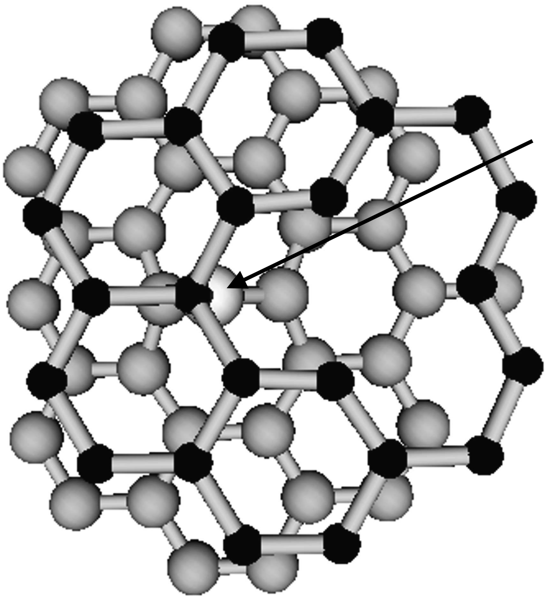

Figure 2. Fragment of BG structure with defect B1 consisting of 57 atoms (plan view). Grey large balls show the bottom graphene plane, black small balls show the top graphene plane. Large light ball shows PKA forming an interlayer bridge (shown by arrow).

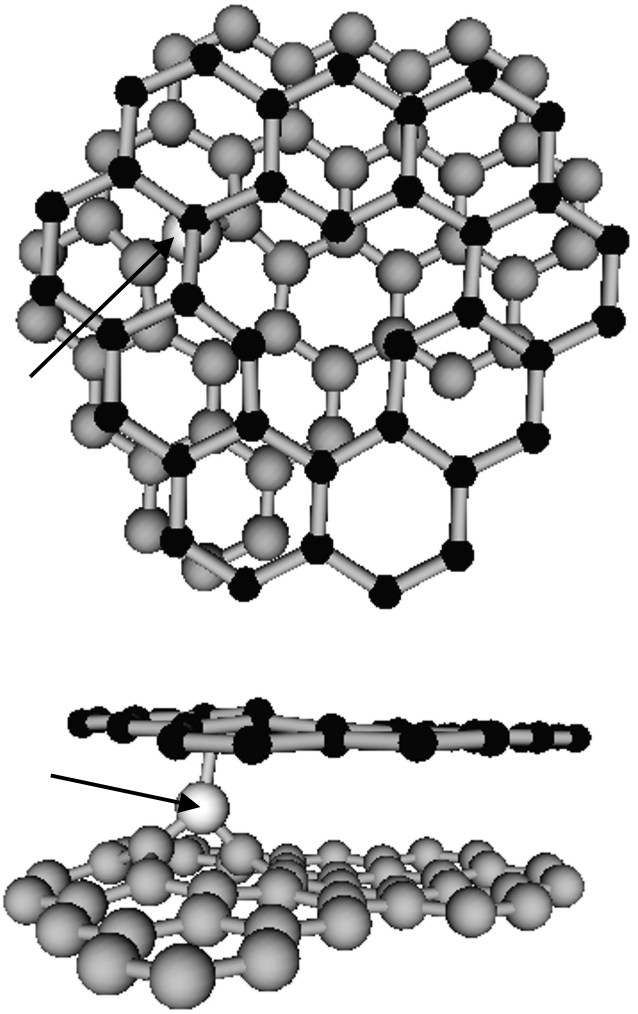

Figure 3. Fragment of BG structure with defect B9 consisting of 80 atoms (plan view and side view). Grey large balls show the bottom graphene plane, black small balls show the top graphene plane. Large light ball shows PKA forming an interlayer bridge (shown by arrow).

The properties of defects with various escape angles and PKA energies are listed in detail in Appendix hereto. Like in [22], the main amount of irradiation-induced interlayer bridges is thermally unstable. From defects listed in table, only defects B1 and B9 with activation energies equal to 1.52 and 2.11 eV, respectively, are of practical interest. Actually, bridge B6 with the third largest activation energy of E_a 1.26 eV has the frequency factor $A = 5 \cdot 10^{14}\,\text{s}^{-1}$. With such parameters, life time of this defect in accordance with expression (1) at 300 and 500 L is equal to 1 month and 0.01 s, respectively. This life time is not sufficient for unstable operation at room temperature. For comparison, annealing frequency factors of defects B1 and B9 (activation energies 1.52 and 2.11 eV) are equal to $2.3 \cdot 10^{14}$ and $2.2 \cdot 10^{13}\,\text{s}^{-1}$. At such values, the annealing times of defects B1 and B9 are equal to, respectively, $1.4 \cdot 10^{11}$ and $1.3 \cdot 10^{22}\,\text{s}$ at $T = 300\,\text{K}$. At $T = 500\,\text{K}$, Radiation-induced defect properties

	Dist (Å)	E_{rel} (eV)	E_a (eV)	N_{coord}	*M* (herein)	*M* ([22])
B1	3.23	12	1.52	C3	3	2
B2	2.74	12.2	1.05	C3	1	0
B3	3.19	12.2	0.99	C3	1	0
B4	1.90	9.5	0.51	C3	11	2
B5	1.99	10.7	0.08	C3	1	0
B6	3.23	12.1	1.26	C3	1	0
B7	1.85	9.9	0.075	C2	4	4
B8	1.92	9.32	0.062	C3	4	1
B9	3.52	12.2	2.11	C3	1	0
B10	1.93	13.1	0.204	C3	1	0
I1	> 4	–	–	C2	5	2
I2	> 4	–	–	C2	52	25
Decay	–	–	–	–	24	20
Total sum					109	56

these values are equal to, respectively, 9 and $8 \cdot 10^7$ s. This stability is sufficient for long-term existence of the bridge at room temperature. Therefore, detailed description of shape is offered only for defect B9 and partial description is provided for defect B1. More detailed description of defect B1 is offered in [22] and the frontal view of this defect is shown in Figure 2. In the unstrained structure, this defect was observed in three irradiation options at $N_r = 2$, $E_0 = 24\,\text{eV}$ with the following angular parameters: $(\Theta/\pi = 4/6,\ \varphi/\pi = 0/4)$; $(\Theta/\pi = 4/6,\ \varphi/\pi = 3/4)$; $(\Theta/\pi = 6/6,\ \varphi/\pi = 0/4)$. Actually, due to a short distance between the interplane bridge and the top graphene plane vacancy $(Dist = 3.23\,\text{Å})$, defect B1 may be treated as a Frenkel pair. Energy properties of tis defect correlate with those of the Frenkel pair defined in accordance with DFT. Thus, in [39], the Frenkel pair energy is within $10.6-13.7\,\text{eV}$ $(12\,\text{eV}$ herein), while the annealing activation energy reported in [40] is equal to $1.3\,\text{eV}$ $(1.52\,\text{eV}$ herein).

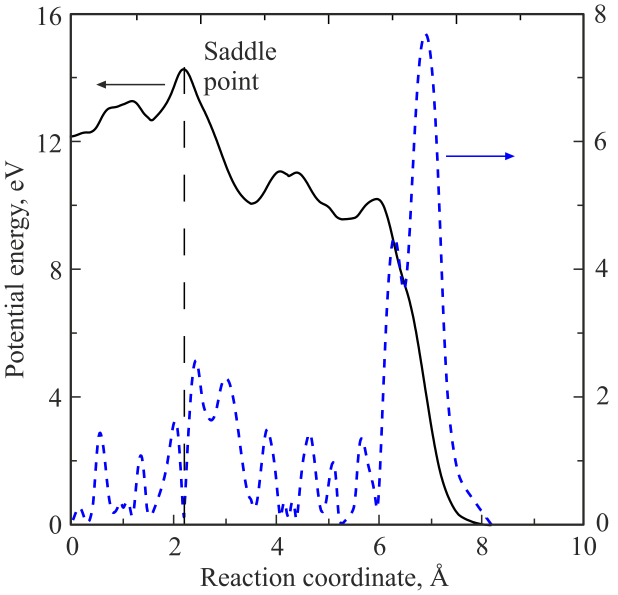

Figure 4. Variation of potential energy and force measure during transformation of BG structure with defect B9 to a defect configuration. Black solid line corresponds to potential energy, blue dashed line corresponds to force measure. Zero energy corresponds to the defect-free configuration energy. Zero response position corresponds to defect B9.

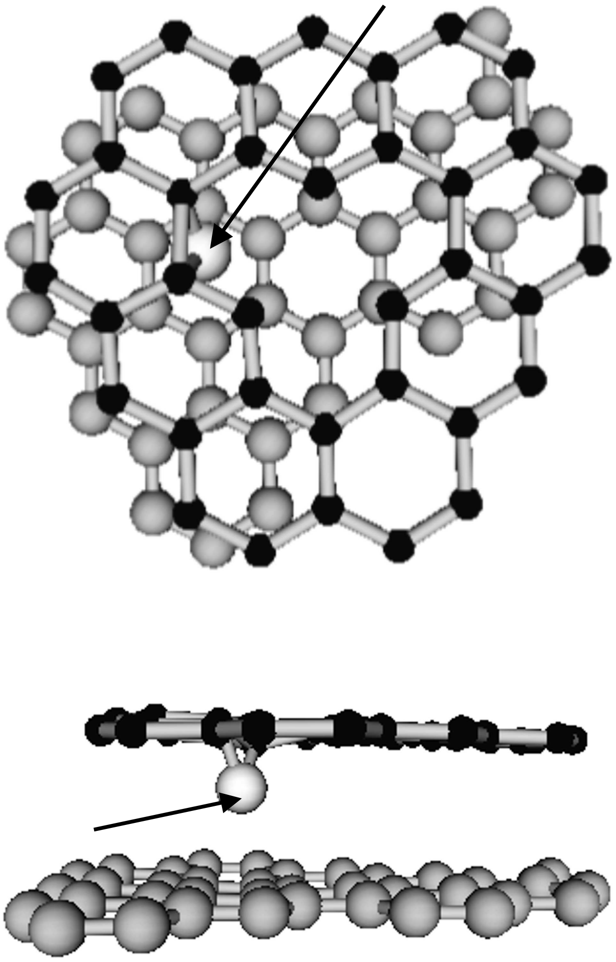

Figure 5. Frontal and side views of the saddle configuration fragment of structure BG with defect B9 consisting of 74 atoms. Designations of atoms are similar to those in Figures 2 and 3.

The most stable defect B9 from those formed during irradiation of the strained BG occurs at the following PKA parameters: $N_r = 2$, $E_0 = 30\,\text{eV}$, $\Theta/\pi = 5/6$, $\varphi/\pi = 0/4$. Shape of this defect is shown in Figure 3. Similarly to configuration B1, PKA forms an interlayer bridge and is covalently bonded by a single bond with a top graphene plane atom. In both defects B1 and B9, PKA in the bottom plane breaks C−C-bond and forms two covalent bonds in its place (see Figure 3). Actually, PKA is an interstitial atom for the bottom plane. In this case, the difference of defect B1 from B9 is in the orientation of the broken bond (see Figures 2 and 3).

Difference in energies E_{rel} of defects B1 and B9 is small (12 and 12.2 eV), however, the annealing activation energies E_a differ considerably (1.52 and 2.11 eV, respectively).

At the optimum path during annealing of defect B9, the BG structure passes through numerous locally stable configurations. Figure 4 shows the dependence of potential energy along the optimum path defined by the chain algorithm described in [36]. The start point of the path corresponds to defect B9, while the end point corresponds to the defect-free configuration. Figure 4 also shows the interatomic force measure in motion along the optimum path. An absolute value of the maximum (by all atoms of the structure) force applied to one atom was chosen as a force measure. Locally stable configurations through which the path goes have minimum points on the potential energy curves shown in Figure 4 and zero (low) force measures. Figure 4 shows that the force measure, in particular, is negligibly low in the initial, final and saddle configurations. The saddle configuration (the point with the maximum energy in Figure 4) defines the annealing activation energy. Analysis of phonon frequencies shows that the initial and final configurations are stable — their spectrum has no imaginary frequencies. The saddle configuration contains a single imaginary frequency equal to 598 cm^{-1}. Form of this saddle configuration is shown in Figure 5. This figure shows that an ideal structure of the bottom graphene plane was restored in the saddle configuration. The atom that served as an interplane bridge has separated from the bottom plane. And the second covalent bond between PKA and the top plane has formed.

4. Conclusion

Comparison of radiation-induced interlayer bridge formation processes in unstressed and stretched BG crystals has shown that two-axis stretching of the structure by 5% increases the radiation-induced defect formation rate significantly. Besides the common defects occurring both in the unstressed structure and in the stretched crystal, formation of a new type of defects was observed during BG deformation. Thus, a thermally stable Frenkel pair with an activation energy of $E_a = 2.11$ eV was detected. Low proportion of these defects that are stable at room temperature compared with the total number of formed defects is a common feature of the radiation-induced interlayer bridge formation processes. Also, regardless of strain, considerable damage near the bridge of both bottom and top graphene planes is a common specific feature of all detected stable bridges.

Acknowledgments

The author is grateful to K.P. Katin for discussion of the findings.

Funding

This study was performed as part of the Program „Priority 2030“ of National Research Nuclear University „MEPhI“.

Conflict of interest

The author declares that he has no conflict of interest.

Appendix

Properties of radiation-induced defects in strained bilayer graphene

Θ/π	N_r	E_0					
φ/π		24 eV	27 eV	30 eV	33 eV	36 eV	39 eV
4/6	1	I2	I2	I2	Decay	Decay	Decay
0/4	2	B1	B2	B3	C4; 5.27	I2	I2
4/6	1	I2	I2	I2	I2	C3; 4.868	I2
1/4	2	B4	I2	I2	B4	I2	I2
4/6	1	I2	I2	I2	I2	I2	I2
2/4	2	I2	I2	I2	I2	I2	I2
4/6	1	0	I2	I2	B5	I2	Decay
3/4	2	B1	I1	I2	I2	I2	I2
4/6	1	I1	I1	B6	I1	I1	C3; 8.07
4/4	2	I2	I2	I2	B7	I2	Decay
5/6	1	B8	0	I2	I2	C3; 4.77	Decay
0/4	2	0	B4	B9*	Decay	Decay	Decay
5/6	1	0	B8	B8	B10	I2	Decay
1/4	2	B4	B4	B4	B4	B4	melt
5/6	1	B8	0	0	I2	I2	I2
2/4	2	B4	B4	B4	I2	I2	I2
5/6	1	0	0	I2	I2	I2	I2
3/4	2	0	0	0	B7	B4	I2
5/6	1	0	0	0	Decay	Decay	Decay
4/4	2	B7	I2	B7	B7	D1	D1
6/6	1	0	0	Decay	Decay	Decay	Decay
0/4	2	B1	Decay	Decay	Decay	Decay	Decay

References

[1] K.S. Novoselov, A.K. Geim, S.V. Morozov, D. Jiang, Y. Zhang, S.V. Dubonos, I.V. Grigorieva, A.A. Firsov. Science **306**, 666 (2004).

[2] K.S. Novoselov, A.K. Geim, S.V. Morozov, D. Jiang, M.I. Katsnelson, I.V. Grigorieva, S.V. Dubonos, A.A. Firsov. Nature **438**, 197 (2005).

[3] A.E. Galashev, O.R. Rakhmanova. UFN, **184** 1045, (2014). (in Russian).

[4] K.A. Krylova, L.R. Safina, R.T. Murzaev, S.A. Shcherbinin, Yu.A. baimova, R.R. Mulyukov. FTT, **65** 1579 (2023). (in Russian).

[5] K.G. Mikheev, R.G. Zonov, N.V. Chuchkalov, G.M. Mikheev. FTT **66**, 280 (2024). (in Russian).

[6] S.Yu. Davydov, FTT **66**, 306 (2024). (in Russian).

[7] S.Yu. Davydov, A.A. Lebedev, FTT, **65** 2048 (2023). (in Russian).

[8] K.G. Mikheev, A.V. Syugaev, R.G. Zonov, D.L. Bulatov, G.M. Mikheev. FTT, **65** 353 (2023). (in Russian).

[9] X. Liu, M.C. Hersam. Sci. Adv. **5** (2019). https://doi.org/10.1126/sciadv.aax6444

[10] A.I. Kochaev, K.P. Katin, M.M. Maslov, R.M. Meftakhutdinov. J. Phys. Chem. Lett. **11**, 5668 (2020).

[11] A.I. Kochaev, M.M. Maslov, K.P. Katin, V. Efimov, I. Efimova. Mater. Today Nano. **20**, 100247 (2022).

[12] L.A. Chernozatonsky, P.B. Sorokin, A.G. Kvashnin, D.G. Kvashnin. Pisma v ZhETF **90**, 144 (2009). (in Russian).

[13] P.V. Bakharev, M. Huang, M. Saxena, S.W. Lee, S.H. Joo, S.O. Park, J. Dong, D.C. Camacho-Mojica, S. Jin, Y. Kwon, M. Biswal, F. Ding, S.K. Kwak, Z. Lee, R.S. Ruoff. Nature Nanotechnol. **15**, 59 (2019).

[14] L.A. Chernozatonskii, K.P. Katin, V.A. Demin, M.M. Maslov. Appl. Surf. Sci. **537**, 148011 (2021).

[15] T. Ohta, A. Bostwick, T. Seyller, K. Horn, E. Rotenberg. Science **313**, 951 (2006).

[16] Y. Zhang, T. Tang, C. Girit. Nature **459**, 820 (2009).

[17] G. Fiori, G. Iannaccone. IEEE Electron Device Lett. **30**, 261 (2009).

[18] M.-C. Chen, C.-L. Hsu, T.-J. Hsueh. IEEE Electron Device Lett. **35**, 590 (2014).

[19] Y. Tang, Z. Liu, Z. Shen. Sens. Actuators B **238**, 182 (2017).

[20] S.Yu. Davydov, FTT **66**, 2050 (2022). (in Russian).

[21] V.A. Demin, D.G. Kvashnin, P. Vancho, G. Mark, L.A. Tchernozatonsky. Pis'ma v ZhETF, **112** 328 (2020). (in Russian).

[22] A.I. Podlivaev. Pis'ma v ZhETF, **117** (456) 2023 (1970). (in Russian).

[23] M.M. Maslov, A.I. Podlivaev, K.P. Katin. Mol. Simulation **42**, 305 (2016).

[24] A.I. Podlivaev, K.S. Grishakov, K.P. Katin, M.M. Maslov. Pis'ma v ZhETF, **113** (182), 2021 (2021). (in Russian).

[25] K.P. Katin, K.S. Grishakov, A.I. Podlivaev, M.M. Maslov. J. Chem. Theory Comput. **16**, 2065 (2020).

[26] K.P. Katin, M.M. Maslov. J. Phys. Chem. Solids **108**, 82 (2017).

[27] L.A. Openov, A.I. Podlivaev. Pisma v ZTEF, **109**, 746 (2019). (in Russian)

[28] A.I. Podlivaev, K.S. Grishakov, K.P. Katin, M.M. Maslov. Pis'ma v ZhETF, **113** 182 (2021). (in Russian).

[29] A.I. Podlivaev, K.S. Grishakov, K.P. Katin, M.M. Maslov. Pis'ma v ZhETF, **114** 172 (2021). (in Russian).

[30] A.I. Podlivaev. Pis'ma v ZhETF, **115** 384 (2022).

[31] K.P. Katin, M.M. Maslov. Mol. Simulation **44**, 703 (2018).

[32] L.A. Openov, A.I. Podlivaev. FTT **57**, 1450 (2015). (in Russian).

[33] A.I. Podlivaev, L.A. Openov. FTT **61**, 604 (2019). (in Russian).

[34] A.I. Podlivaev. Pis'ma v ZhETF, **111** (728) 2020). (in Russian).

[35] E.M. Pearson, T. Halicioglu, W.A. Tiller. Phys. Rev. A **32**, 3030 (1985).

[36] K.P. Katin, A.I. Podlivaev, A.I. Kochaev, P.A. Kulyamin, Y. Bauetdinov, A.A. Grekova, I.V. Bereznitskiy, Mikhail M. Maslov. Flat Chem., **44**, 100622 (2024). https://doi.org/10.1016/j.flatc.2024.

[37] G.V. Vineyard. J. Phys. Chem. Solids. **3**, 121 (1957).

[38] A.A. El-Barbary. Appl. Surf. Sci. **426**, 238 (2017).

[39] S.B. Isbill, A.E. Shields, D.J. Mattei-Lopez, R.J. Kapsimalis, J.L. Niedziela. Comput. Mater. Sci. **195**, 110477 (2021).

[40] C.P. Ewels, R.H. Telling, A.A. El-Barbary, M.I. Heggieand P.R. Briddon. Phys. Rev. Lett. **91**, 025505 (2003).

Translated by E.Ilinskaya